

## Cathodic Protection Criteria for X80 Steel in Soil Extract

Shixiong Wu<sup>1</sup>, Zhiming Gao<sup>1,\*</sup>, Jun Zhao<sup>2</sup>, Liqin Wang<sup>3</sup>, Yingjie Liu<sup>1</sup>, Meijun Wu<sup>1</sup>, Wenbin Hu<sup>1</sup>

<sup>1</sup> School of Material Science and Technology, Tianjin University, Tianjin, 30072, China  
Engineering Research Center of Composite and Functional Materials, Ministry of Education, Tianjin, 30350, China

<sup>2</sup> Petrochina pipeline company oil&gas storage and transportation technology sub-company, Langfang, 065000, China

<sup>3</sup> Amperex Technology Limited, Ningde, 352100, China

\*E-mail: [gaozhiming@tju.edu.cn](mailto:gaozhiming@tju.edu.cn)

*Received: 25 August 2019 / Accepted: 30 October 2019 / Published: 30 November 2019*

---

Potentiodynamic polarization, electrochemical impedance spectroscopy and slow strain tensile rate tests were used to establish the negative critical potential range for cathodic protection of X80 steel in soil extract. The results showed that the hydrogen-charged potential was around -800 mV (vs. SCE), and the applied cathodic potential was of great significance for X80 steel's hydrogen embrittlement. Besides, when the cathodic protection potential was in the range prior to -850 mV, the amount of hydrogen evolution was insignificant, which had a little effect on the mechanical performance of X80 steel. Meanwhile, the fracture morphology showed dimple-like plastic fracture characteristics. On the contrary, with negative shift of the cathodic potential to -900 mV or more, a plastic brittle transition occurred owing to the large amounts of hydrogen released at this time. Thus, the negative critical potential range of X80 steel during the cathodic protection process at room temperature in soil extract was determined as -800 mV ~ -850 mV.

---

**Keywords:** API X80 steel, potentialdynamic polarization, EIS, SSRT, hydrogen embrittlement

### 1. INTRODUCTION

With the increasing demand for energy and its uneven distribution, pipeline steel is playing an increasingly important role in oil and gas transportation[1-5]. In recent years, the pipe coefficient gradually changed from 0.72 to 0.8, which necessitates new requirements for steel strength. API X80 steel stands out as the preferred steel grade for pipeline steel in the 21st century due to its optimal comprehensive performance. For instance, it has been widely applied in China's west-east gas transmission project[6-8].

Corrosion failure, a common failure mode of pipeline steel, occurs frequently owing to the severe service environment of the long-distance transportation pipelines. Substantial research studies have been performed to explore the corrosion inhibition methodologies[9-10]. Cathodic protection, combined with organic coatings, is a widely used method to achieve long-term protection of pipeline steel[11-12]. It should be particularly assessed whether the applied cathodic protection potential is appropriate. If the protective potential is too positive, the material cannot be adequately protected and corrosion must occur. Otherwise, overprotection may lead to hydrogen evolution, thus, resulting in hydrogen embrittlement[13-18].

It is not clear if the cathodic protection criterion currently proposed (i.e., -850 mV~-1200 mV vs. CSE) for low strength steel is suitable for API X80 steel, which has a higher sensitivity to hydrogen embrittlement. Therefore, studies in relation to the cathodic protection system and hydrogen embrittlement sensitivity of X80 in soil extract are urgently needed to establish the cathodic protection criteria [19-20].

## 2. EXPERIMENTAL PROCEDURES

### 2.1. Materials and sample preparation

The soil was taken from 1.5 m underground, where pipeline was buried, in Chang-ling of Ji-Lin Province. The extracted soil solution was prepared by mixing soil with distilled water in the mass ratio 1:1. Before experiments, chemical analysis was carried out to determine the soil chemistry and the results are shown in Table 1.

**Table 1.** Chemical composition of the extracted soil solution (mol/L)

CO <sub>3</sub> <sup>2-</sup>	HCO <sub>3</sub> <sup>-</sup>	SO <sub>4</sub> <sup>2-</sup>	Cl <sup>-</sup>	Ca <sup>2+</sup>	Mg <sup>2+</sup>	Na <sup>+</sup>	K <sup>+</sup>	pH
<0.025	1.65	0.11	0.05	1.74	0.49	0.22	0.09	6.50

The experiment was carried on the X80 steel samples, the composition of which has been shown in Table 2. The specimens used for electrochemical tests were cut into 10\*10\*5 mm and were embedded with epoxy resin, leaving a working area of 1cm<sup>2</sup>. The size of the tensile sample is shown in Fig. 1 with a thickness of 2 mm. All the specimens were abraded up to 2000 grit using SiC paper to guarantee the same surface condition, and then blow-dried after rinsed with distilled water and ethanol.

**Table 2.** Chemical composition of X80 pipeline steel (wt.%)

C	Si	Mn	P	S	Cr	Mo	Ni	Cu	V	Nb	Ti	Fe
0.047	0.19	1.85	0.013	<0.008	0.22	0.15	0.25	0.24	0.0041	0.082	0.018	Balance

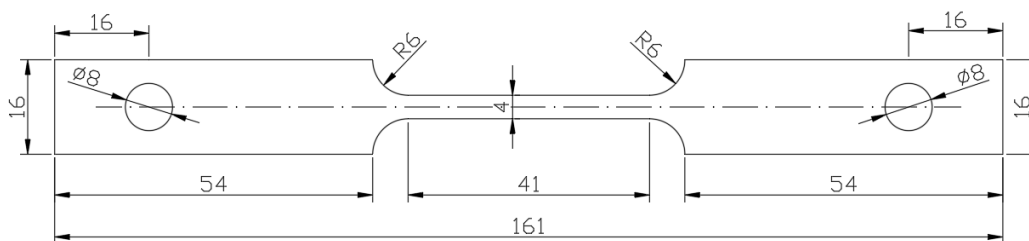


**Figure 1.** Shape and size of the tensile specimen (in mm)

## 2.2. Polarization and electrochemical impedance spectroscopy measurements

Electrochemical measurements are effective methods used to study the corrosion behavior of metal. The tests were conducted by using a PARSTAT 2273 electrochemical workstation with a three-electrode system, where the saturated calomel electrode served as reference electrode, platinum plate as auxiliary electrode, and X80 steel as working electrode. Prior to each test, the sample was immersed in the prepared soil extract for approximately 1 hour to stabilize the electrode system.

The potentialdynamic polarization scanned from -0.5 V to 0.8 V (vs.OCP) with a rate of 0.1667 mV/s. Electrochemical impedance spectroscopy tests at different polarization potentials were performed with sinusoidal perturbations which scanned from 10 kHz to 0.01 Hz with an amplitude of 10 mV. The specimens were polarized for 10 min at the corresponding potential before test.

## 2.3. Slow strain rate tensile test

The slow strain rate tensile test was used to investigate the hydrogen embrittlement sensitivity of X80 steel at different cathodic protective potential by the Cor-Force Stress-Corrosion Test Equipment. The strain rate was set as  $10^{-6}$ /s, and a tensile test performed in air medium was used as a blank and control group. The tensile experiments conducted at different cathodic potentials were all polarized for 6 h in advance at the corresponding cathodic potential before loading to ensure the hydrogens generated have enough time to diffuse into the samples. Finally, the fracture of the slow strain rate tensile specimen was cut off was cleaned with a special water-based chemical cleaner, then the fractographic features was obtained by scanning electron microscope.

## 3. RESULTS AND DISCUSSION

### 3.1. Determination of the actual hydrogen evolution potential of X80 steel in soil extract.

The polarization curves obtained from the experiment conducted at room temperature in the soil extract are shown in Fig. 2. It is can be seen that the open-circuit-potential of X80 is around - 640 mV at this condition, and two inflection points A and B are observed in the cathodic polarization curve. The cathodic reaction is mainly controlled by the oxygen activation reaction before point A, whereas it is

controlled by oxygen diffusion in the range of potential between A and B. With the negative shift of the cathodic potential, the hydrogen depolarization reaction becomes obvious, which acquires a larger proportion in the whole cathodic reaction.

As the applied cathodic potential is varied in the range from A to B, hydrogen evolution reaction is still very weak, and the potential change with impressed current is obvious, along with the cathodic protection potential generally selected in this range. In addition, hydrogen evolution reaction begins to occur at the potential earlier than point B, as pointed out in research reports of Gao [21,22]. Hence, potential corresponding to the point B can be termed as the apparent hydrogen evolution potential here to distinguish from the actual hydrogen-charged potential.

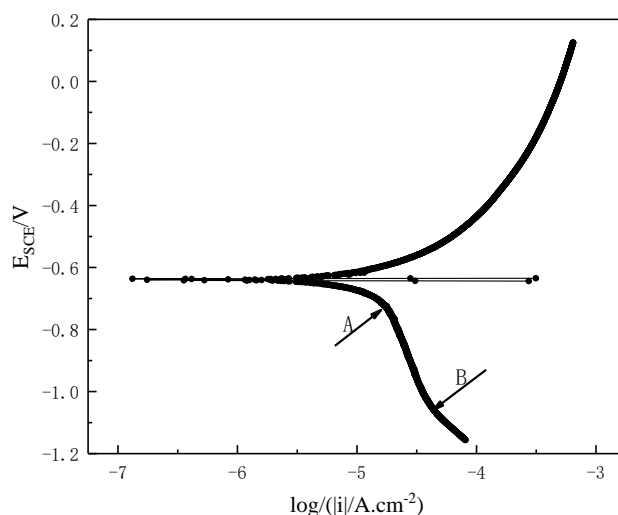


**Figure 2.** Potentiodynamic polarization curve of X-80 at room temperature in soil extract

Electrochemical impedance spectroscopy was performed under open-circuit potential and different cathodic polarized potentials within the potential range during which the diffusion of oxygen controls the whole cathodic reaction, thus, resulting in the appearance of the limiting current density in the cathodic polarization curve (i.e, the potential range from A to B). The electrochemical impedance spectroscopy data was fitted with ZSimpWin using the equivalent circuit shown in Fig. 3, where  $R_s$  is the solution resistance,  $Q_f$  and  $R_f$  represent the adsorption capacitance and resistance of corrosion products respectively,  $Q_{dl}$  refers to the double layer capacitance and  $R_t$  is the charge transfer resistance. The resulting findings are shown in Fig. 4.

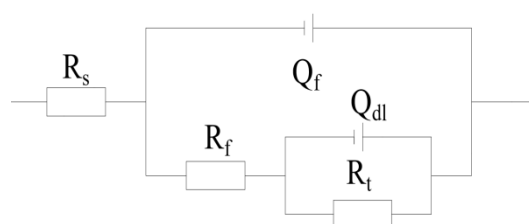


**Figure 3.** Equivalent circuit used for X-80 at room temperature in soil extract

According to the theory of impedance spectrum, the anode and cathode reactions occur simultaneously. Therefore, the data measured by electrochemical impedance spectrum originates from two reactions in parallel, namely  $1/R_t=1/R_{ta}+1/R_{tc}$ , where  $R_{ta}$  represents the charge transfer resistance of the anode reaction and  $R_{tc}$  represents the charge transfer resistance of the cathode reaction. The anode reaction is gradually suppressed with the negative shift of the cathode polarization potential before hydrogen evolution potential, while the cathode reaction is mainly controlled by oxygen diffusion at this time, thus, the potential has a little influence on it. As the potential is further shifted to negative side, the hydrogen depolarization reaction occurs, and the more negative the potential is, the easier it is to carry out the reaction. Therefore, in the impedance spectrum test results, the charge transfer resistance first increases and subsequently decreases with the negative shift of potential. There is a peak potential in the whole process, which is the actual hydrogen evolution potential of the corrosion system [21-23].

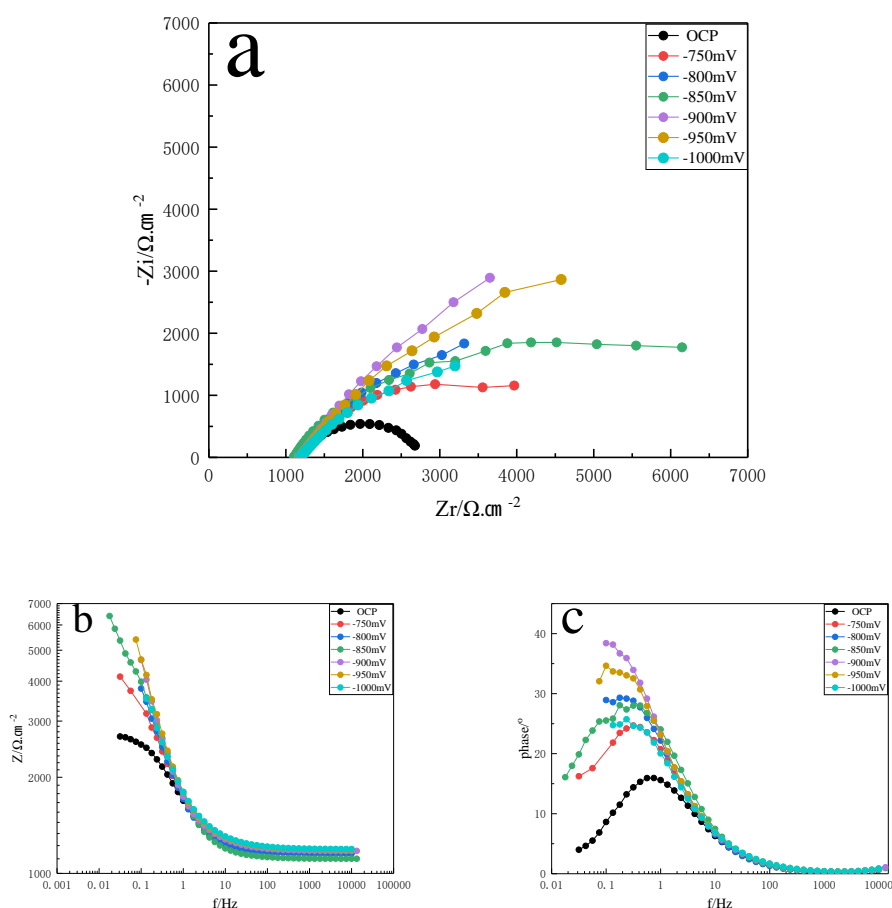


**Figure 4.** The EIS of X-80 under different cathodic polarization potential at room temperature in soil extract

According to the above theory, Fig. 5 indicates that the actual hydrogen evolution potential of X80 steel in soil extract at room temperature is approximately -800 mV, rather than the value of -1000 mV corresponding to the potential of inflection point B in the cathodic polarization curve. Besides, it can also be seen in Fig. 4 that the arc radius of Nyquist diagram and module value increase with the negative shift of potential before hydrogen evolution potential and subsequently decrease gradually. In

the phase diagram, the characteristic frequency also moves towards lower frequencies at first, followed by the shift towards higher values, which is bounded by the hydrogen evolution potential.

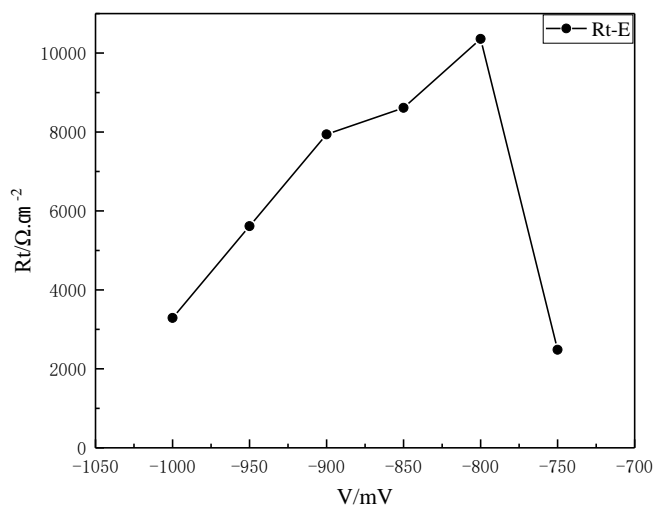


**Figure 5.** The  $R_t$  vs.  $E$  curves of X-80 at room temperature in soil extract

### 3.2 Exploration of the effect of polarization potential on mechanical properties

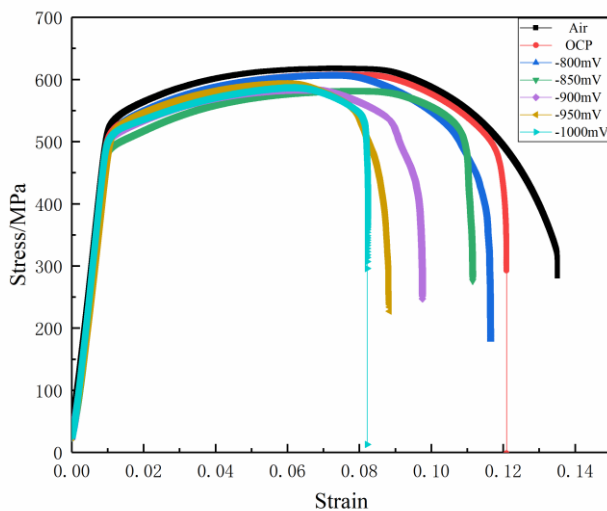


**Figure 6.** Stress–strain curves of X-80 steel specimens in air and in soil extract under different cathodic potential

The slow strain rate tensile test is used to study the influence of cathodic polarization level on the mechanical properties of X80 steel at room temperature in soil extract. The results are shown in Fig. 6 and Table 3. It is observed that the stress-strain curves have no obvious change in elastic strain stage under different cathodic potentials. However, the mechanical properties of materials decline rapidly with

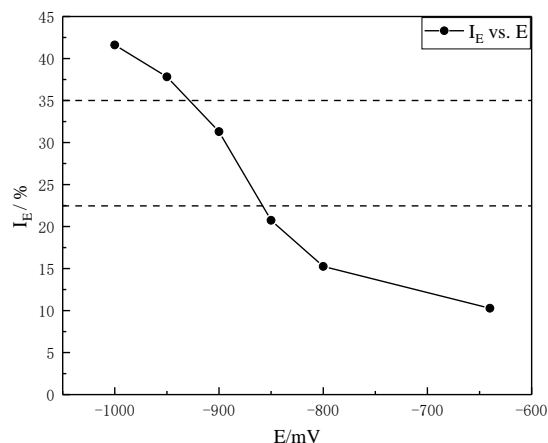
the negative shift of the applied potential after tensile strength. In order to describe the degree of loss of the mechanical properties in detail, the fracture energy loss rate  $I_E$  of the tensile samples was taken as the stress corrosion cracking susceptible index of X80 steel.  $I_E$  is defined as follows:

$$I_E = 1 - \frac{E_e}{E_0} \times 100\% \quad (1)$$

**Table 3.** Mechanical property parameters of X80 tensile experiment with slow strain rate under different protection potentials

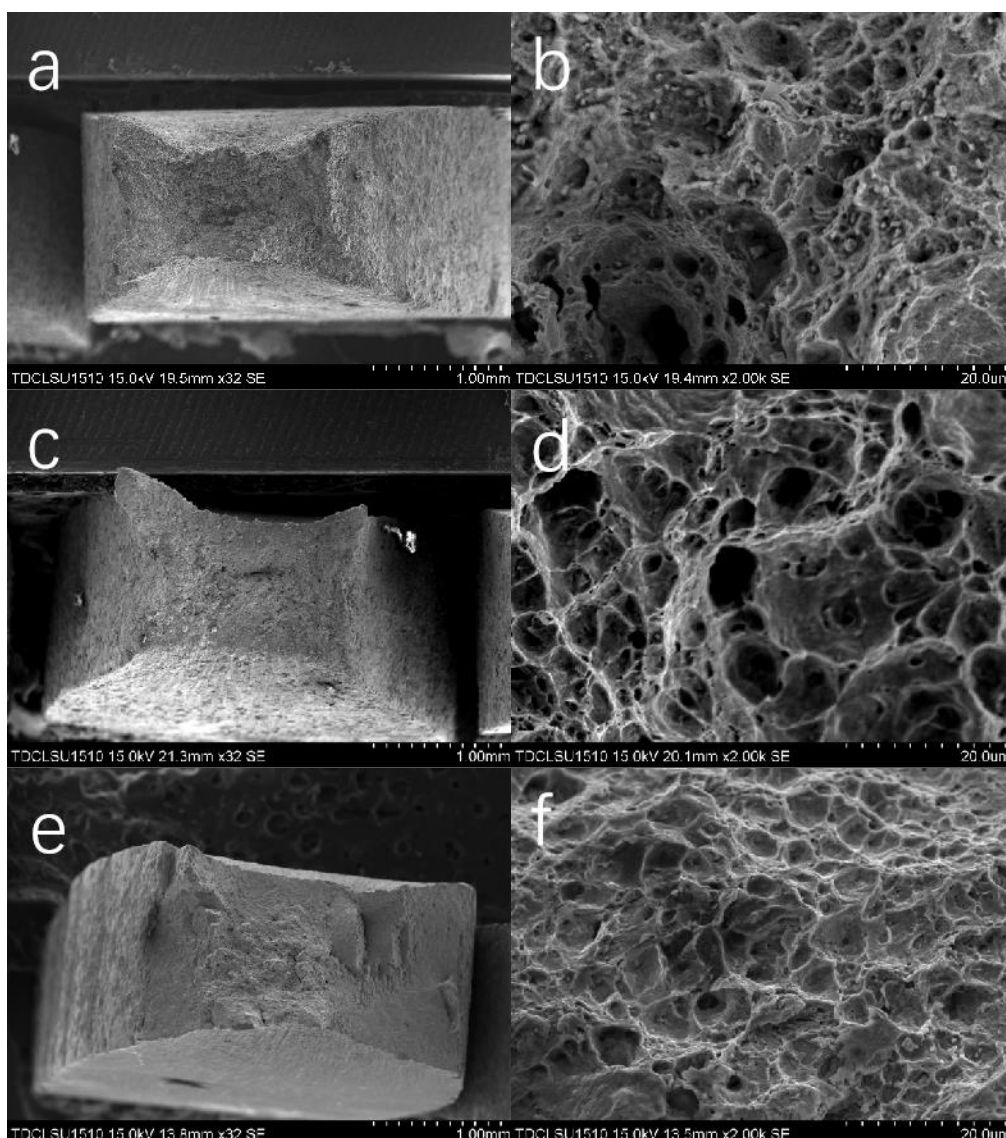
$E/V$	$\sigma_b/MPa$	$\sigma_s/MPa$	Fracture Energy / (J.cm <sup>-2</sup> )	$\delta /%$	$\psi/%$	$I_E/%$
Air	618.05	526.99	73.97	13.51	76.11	..
OCP	607.79	523.78	66.37	12.09	41.55	10.28
-0.8	593.47	524.58	62.68	11.65	37.10	15.25
-0.85	582.85	495.75	58.62	11.15	24.35	20.74
-0.90	583.56	510.98	50.82	9.75	33.58	31.29
-0.95	593.34	530.00	45.00	8.84	26.13	37.82
-1.00	587.01	512.43	43.19	8.22	14.01	41.61

where  $E_e$  is the fracture energy obtained from the test and  $E_0$  represents the fracture energy in the blank test (i.e. in air). As suggested by Kong [24], the susceptibility of a material to hydrogen embrittlement increases with the value of stress corrosion cracking susceptible index  $I_E$ . Besides, the empirical criterion for evaluating the susceptibility to HE put forward in the study by Kong, along with explaining the decreased mechanical properties of X80 in simulated deep sea environment [25], was also employed in the present study. As is shown in Fig. 7, when  $I_E$  is less than 25% before -850 mV, the material exhibits good plasticity, thus, it is safe for X80 steel to serve under these conditions. However, as  $I_E$  is in the range between 25% and 35%, the material presents the risk of embrittlement failure. Furthermore, as the potential is moved negatively to -950mV, the  $I_E$  is greater than 35%, and it can be confirmed that the embrittlement failure would occur as accident.



**Figure 7.** The fracture energy loss of X-80 vs.  $E$  curves in soil extract under different cathodic potential.

Moreover, the fracture surface of the samples after slow strain rate tensile test was analyzed by SEM, facilitating direct observation of the fracture morphology and reflecting the reliability of the stress corrosion cracking susceptible index  $I_E$ . As described in Fig.8, the fracture morphologies show dimple pattern with features of plastic fracture ahead of the potential value of -850 mV. The dimples are observed to become smaller and shallower gradually with further negative shift of potential, indicating that the susceptibility to SCC increased with decreased potential. As the potential is below -900 mV, a brittle cleavage fracture is observed as expected. Overall, the fracture surface analysis concluded the same results represented by index  $I_E$ .



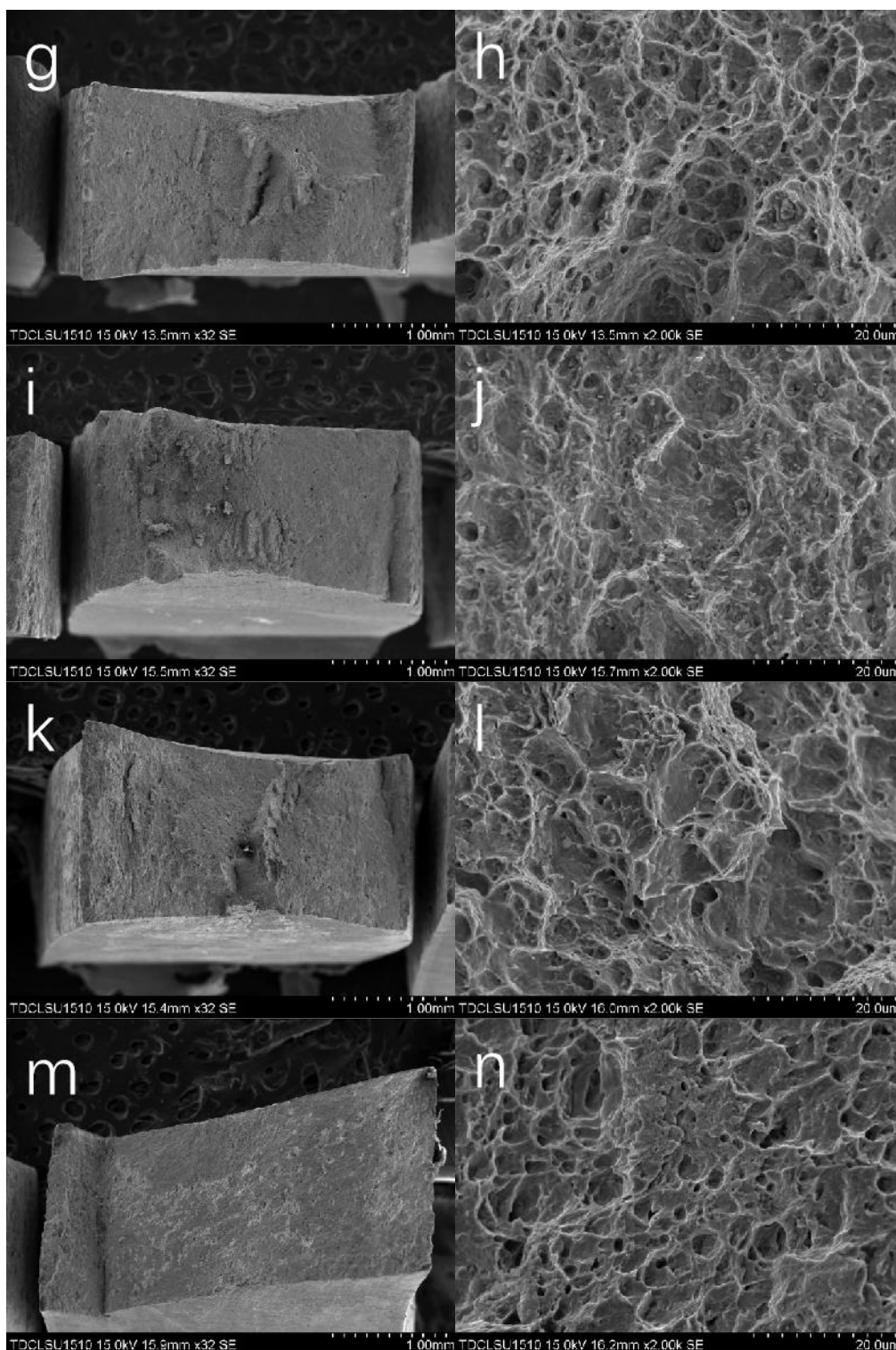


**Figure 8.** The SEM micrograph of the fracture surface of X-80 in air without protection (a and b) and in soil extract under the potential ranging from *OCP* to -1000mV (c -n) at room temperature

From the above discussion, it can be suggested that the cathodic polarization has obvious influence on the mechanical properties of X80 steel. In case the potential is above -850 mV, the fracture surface is characterized by ductile rupture, showing low SCC sensitivity, due to the reason that the anodic dissolution is inhibited, similar to the findings of Liu on the mechanism of X70 in an acidic soil

environment [26]. Meanwhile, a small amount of hydrogen evolution has a little effect on the mechanical loss of materials [25]. However, as the potential decreased to -900 mV, the brittle fracture feature appears with the value of  $I_E$  lower than 25%. With the negative shift of the cathodic potential, the SCC sensitivity of X80 steel is observed to increase by degrees, as analyzed from the fracture morphology and  $I_E$ . This is mainly due to the reason that an excessive cathodic polarization can lead to the occurrence of hydrogen evolution, and the generated hydrogen atoms will adsorb on the surface of the sample, followed by permeation. Thus, the surface energy of steel is reduced for hydrogen adsorption and crack initiation becomes easier with applied stress, and the hydrogen atoms entering the interior of the matrix metal will accumulate and induce decohesion at the interfaces of different structures. Furthermore, the dislocation can carry the hydrogen atoms to the crack tip for enrichment, reaching the critical concentration of hydrogen-induced plastic deformation as the tensile was loaded. Both mechanisms are likely to cause a certain damage to the mechanical properties of X80 steel, similar to the analysis reported in other literature studies [19,25].

It can be concluded that the selection of a suitable cathodic protective potential is a critical factor in improving the corrosion resistance of X80 steel without loss of mechanical performance. In the present study, the negative critical value of the potential, which would be applied on X80 steel in the process of cathodic protection at room temperature in soil extract, is determined in the range of -800~-850 mV (vs. SCE). The upper limit of the applied cathodic potential region is still selected as -850 mV (CSE) (in the whole process, the ohm drop is ignored because its value is smaller than the potential interval during the study).

#### 4. CONCLUSION

Cathodic protection criteria for X80 steel in soil extract was studied via potentiodynamic polarization, electrochemical impedance spectroscopy and slow strain tensile rate tests combined with fracture morphology. The main results are summarized as follows:

(1) The actual hydrogen evolution potential of X80 steel at room temperature in the soil extract is about -800 mV, which is different from the value obtained from the polarization curve conventionally.

(2) In case the potential is in the range prior to -850 mV,  $I_E$  is less than 25% with fracture appearance showing the characteristics of plastic dimples, thus, indicating low susceptibility to stress corrosion cracking, though there might have been a small amount of hydrogen evolution at this stage.

(3) As potential decreases to -900 mV or more, the sensitivity of X80 steel to hydrogen embrittlement increases gradually, which can be gauged from the high value of  $I_E$  with features of quasi-cleavage fracture observed during SEM morphology analysis.

(4) The degradation of mechanical properties of X80 under cathodic protection is mainly caused by the generated hydrogen, which can adsorb on the surface and reduce surface energy, or diffuse into material for enrichment to the critical concentration required to induce decohesion at the interfaces of different structures and additional plastic deformation with the help of dislocation motion.

(4) The negative critical potential range of cathodic protection for X80 can be determined approximately in the range -800~-850 mV ( vs. SCE) under the condition explored in this study.

## ACKNOWLEDGMENTS

This research is supported by National Natural Science Foundation of China (No.51871164, No. 51671144), Tianjin science and technology program (No.18YFZCGX00050) and Shandong Taishan Industry Leading Talents Project (No.SF1503302301).

## References

1. S. Y. Han, Y. S. Sang, C. H. Seo, H. Lee, J. H. Bae, K. Kim, *Metall. Mater. Trans. A*, 40 (8) (2009) 1851.
2. W. Zhao, T. Zhang, Y. Zhao, J.B. Sun, W. Yong, *Corros. Sci.*, 111 (2016) 84.
3. L. Li, B. Song, J. Cheng, Z. Yang, Z. Cai, *Int. J. Hydrogen Energy*, 43 (2018) 17353.
4. Z. X. Yao, S. Jiang, G. Wang, L. Yin, D. Jiang, Z. Zhang, *Int. J. Electrochem. Sci.*, 14 (2019) 2672.
5. B.A. Shaw, R.G. Kelly, *Electrochem. Soc. Interface*, 15 (2006) 24.
6. W. Zhou, W. Lan, X. L. Cao, H. D. Deng, Y. B. Yan, X. L. Hou, *Int. J. Electrochem. Sci.*, 13 (2018) 1283.
7. B. He, C. H. Lu, P. J. Han, X. H. Bai, *Eng. Fail. Anal.*, 59 (2016) 410.
8. P. Liang, X. Li, C. Du, X. Chen, *Mater. Design*, 30 (2009) 1712.
9. J. G. Gonzalez-Rodriguez, M. Casales, V. M. Salinas-Bravo, J. L. Albarran, L. Martinez, *Corrosion*, 58 (2002) 584.
10. M. Dai, J. Liu, F. Huang, Y. Zhang, Y. F. Cheng, *Corros. Sci.*, 143 (2018) 428.
11. M. Barbalat, D. Caron, L. Lanarde, *Corros. Sci.*, 73 (2013) 222.
12. M. Barbalat, L. Lanarde, D. Caron, *Corros. Sci.*, 55 (2012) 246.
13. H. Addach, P. Berçot, M. Rezzazi, *Corros. Sci.*, 51 (2009) 263.
14. N. E. Nanninga, Y. S. Levy, E. S. Drexler, *Corros. Sci.*, 59 (2012) 1.
15. S. Komazaki, R. Maruyama, T. Misawa, *ISIJ Int.*, 43 (2003) 475.
16. M. Cabrini, S. Lorenzi, P. Marcassoli, *Corros. Rev.*, 29 (2011) 261.
17. C. Batt, J. Dodson, M. J. Robinson, *BRIT CORROS J*, 37 (2002) 194.
18. R. Thodla, M.T. Piza Paes, B. Gerst, *Int. J. Hydrogen. Energy*, 40 (2015) 17051.
19. I. Moro, L. Briottet, P. Lemoine, *Mater. Sci. Eng., A*, 527 (2010) 7252.
20. Y. Liu, Z. Gao, X. Lu, L.Q. Wang, *Int. J. Electrochem. Sci.*, 14 (2019) 150.
21. Z. Gao, X. Liu, L. Wen, W. Kang, *Int. J. Electrochem. Sci.*, 11 (2016) 3007.
22. Z. M. Gao, Y. Y. Liu, F. Lin, L. H. Dang, L. J. Wen, *Int. J. Electrochem. Sci.*, 8 (2013) 10446.
23. M. Orazem, B. Tribollet, *Electrochemical impedance spectroscopy*, John Wiley & Sons, (2017) Hoboken, US.
24. D. Kong, Y. Wu, L. Dan, *J. Iron Steel Res. Int.*, 20 (2013) 40.
25. Y. Liu, Y. L. Q. Li, *Acta Metall. Sinica*, 49 (2013) 1089.
26. Z. Y. Liu, X. G. Li, C. W. Du, *Corros. Sci.*, 50 (2008) 2251.

© 2020 The Authors. Published by ESG ([www.electrochemsci.org](http://www.electrochemsci.org)). This article is an open access article distributed under the terms and conditions of the Creative Commons Attribution license (<http://creativecommons.org/licenses/by/4.0/>).